

An alternative differential method of femtosecond pump-probe examination of materials

R. Ivanov,^{1,*} Jesús Villa,² Ismael de la Rosa,² and E. Marín³

¹Facultad de Física, Universidad Autónoma de Zacatecas, Calz. Solidaridad Esquina Paseo de la Bufa s/n, C. P. 98060, Zacatecas, Zac., Mexico

²Laboratorio de Procesamiento Digital de Señales, Facultad de Ingeniería Eléctrica, Universidad Autónoma de Zacatecas, Avenida Ramón López Velarde 801, Zacatecas 98000, Mexico

³Centro de Investigación en Ciencia Aplicada y Tecnología Avanzada, Instituto Politécnico Nacional, Legaría 694, Colonia Irrigación, C. P. 11500, Mexico D. F., Mexico

rumen5252@yahoo.com.mx

Abstract: We describe an alternative method for femtosecond pump-probe beam examination of energy transport properties of materials. All already reported techniques have several drawbacks which limit precise measurements of reflection coefficient as function of time. A typical problem is present when rough samples are being studied. In this case the pump-beam polarization changes randomly which may produce a spurious signal, drastically reducing the signal to noise ratio. Some proposals to alleviate such problem have been reported, however, they have not been totally satisfactory. The method presented here consists on measuring the difference between the two delays' signals of the probe-beam. As will be explained, our proposal is free of typical drawbacks. We also propose a numerical method to recover the $\Delta R(t)/R$ curve from the measured data. Numerical simulations show that our proposal is a viable alternative.

© 2011 Optical Society of America

OCIS codes: (320.2250) Femtosecond phenomena; (320.7090) Ultrafast laser; (320.7100) Ultrafast measurements; (120.5700) Reflection; (260.7120) Ultrafast phenomena.

References and links

1. P. M. Norris, A. P. Caffrey, R. J. Stevens, J. M. Klop, J. T. McLeskey Jr., and A. N. Smith, "Femtosecond pump-probe nondestructive examination of materials," *Rev. Sci. Instrum.* **74**, 400–406 (2003).
2. G. A. Antonelli, B. Perrin, B. C. Daly, and D. G. Cahill, "Characterization of mechanical and thermal properties using ultrafast optical metrology," *MRS Bull.* **31**, 607–613 (2006).
3. K. L. Hall, G. Lenz, E. P. Ippen, and G. Raybon, "Heterodyne pump-probe technique for time-domain studies of optical nonlinearities in waveguides," *Opt. Lett.* **17**, 874–876 (1992).
4. K. Yokoyama, C. Silva, D. H. Son, P. K. Walhout, and P. F. Barbara, "Detailed investigation of the femtosecond pump-probe spectroscopy of the hydrated electron," *J. Phys. Chem. A* **102**, 6957–6966 (1998).
5. H.-C. Wang, Y. C. Lu, C. Y. Chen, C. Y. Chi, S. C. Chin, and C. C. Yang, "Non-degenerate fs pump-probe study on InGaN with multi-wavelength second-harmonic generation," *Opt. Express* **13**, 5245–5251 (2005).
6. J. Zhang, A. Belousov, J. Karpinski, B. Batlogg, and R. Sobolewski, "Femtosecond optical spectroscopy studies of high-pressuregrown (Al,Ga)N single crystals," *Appl. Phys. B: Lasers Opt.* **29**, 135–138 (1982).
7. Illingworth and I. S. Ruddock, "The analysis of excite and probe measurements of relaxation times with fluctuating pulse duration," *Appl. Opt.* **43**, 6139–6146 (2004).
8. S. V. Rao, D. Swain, S. P. Tewari, "Pump-probe experiments with sub-100 femtosecond pulses for characterizing the excited state dynamics of phthalocyanine thin films," *Proc. SPIE* **7599**, 75991P (2010).

9. A. Yu, X. Ye, D. Ionascu, W. Cao, and P. M. Champion, "Two-color pump-probe laser spectroscopy instrument with picosecond time-resolved electronic delay and extended scan range," *Rev. Sci. Instrum.* **76**, 114301 (2005).
10. K. Kang, Y. K. Koh, C. Chiritecu, X. Zheng, and D. G. Cahill, "Two-tint pump-probe measurements using a femtosecond laser oscillator and sharp-edged optical filters," *Rev. Sci. Instrum.* **79**, 114901 (2008).
11. B. Bousquet, L. Canioni, J. Plantard, and L. Sarger, "Collinear pump probe experiment, novel approach to ultrafast spectroscopy," *Appl. Phys. B: Lasers Opt.* **68**, 689–692 (1999).

1. Introduction

The pump-probe beam method with femtoseconds pulsed lasers is a powerful tool to investigate energy transport properties of materials, such as thin films [1], nanostructures [2], waveguides [3], chemical processes [4], etc. A description of the typical setup for transient thermoreflectance and thermotransmission technique can be found in Ref. [1]. Figure (1) shows the temporal dependent $\Delta R(t)/R$, induced by laser heating. The constant term R represents the optic-reflection coefficient while the time dependent $\Delta R(t)$ represents the optic-reflection coefficient due to the pump-beam ($\Delta R(t) \ll R$).

The method reported in [1] works in the following way: A pulse train from the pump-beam is

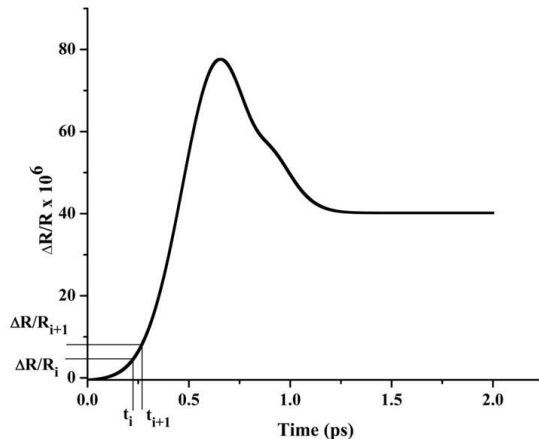


Fig. 1. Time dependent $\Delta(t)/R$ function (29 nm Pt/Si sample, photon wavelength= 757 nm).

modulated through the acousto-optic modulator. This beam impinges on the sample changing its reflection coefficient. This time dependent change is measured with the probe-beam. The probe-beam's amplitude changes as $\Delta R(t)/R$ does due to the pulse delay variations realized by means of the displacements of the dove prism. The probe-beam crosses the polarizer whose polarization plane is oriented such that scattered pump-beam is attenuated, and probe-beam goes to the photo-detector. The averaged signal generated by the photo-detector is measured with the help of a lock-in amplifier. In this way the $\Delta R(t)/R$ curve is generated.

This method [1] have two main drawbacks. (1) The time resolution is equal or less than the pump-beam period. To increase the time resolution some authors have proposed the use of shorter pulsed lasers (down to 10 fs [5]), which could be a very expensive alternative. (2) As the Lock-in amplifier is synchronized at the pump-beam modulation frequency, another drawback is that when rough samples are studied, scattered light can not be eliminated by the polarizer which causes a low signal to noise ratio. There are several already reported methods to reduce

this drawback which consist on separate the pump-beam and the probe-beam, duplicating the pump-beams' frequency and using filters to eliminate the scattered light [6, 7], using tunable lasers [8], using two synchronized lasers of different wave-lengths [9], using different parts of a beam's spectrum as pump-beam and sensor [10], and other interesting proposals [11]. These methods, however, are so expensive and/or they do not completely eliminate the drawback.

2. Description of the alternative method

Unlike already reported methods, which modulate the pump-beam, our method depends on sine modulation of the probe-beam delay. In this way the lock-in amplifier detects the voltage amplitude given by the photodiode, which corresponds to the difference $\Delta R/R_{i,i+1} = \Delta R/R_{i+1} - \Delta R/R_i$. In Fig. (2) we show the experimental setup for this purpose. The laser (for example, MIRA-HP, Coherent) emits a pulsed beam with the following characteristics: pulse duration ~ 190 fs, frequency=76 MHz, wave-length= 720 – 880 nm, mean optical power= 1.2 W. Light passes through the beamsplitter (for example, NT31-416, Edmund), pump-beam crosses through a variable gray filter (for example, NT63-048, Edmund), a lens focuses the pump-beam on the sample. The probe-beam passes through a variable gray filter and a $\lambda/2$ plate to turn 90° its polarization plane, it is reflected by the vibrant reflector (for example, Broadband Hollow Retroreflector, model: UBBR2.5-1S, Newport) and reaches the sample. The vibrant reflector is coupled with a piezoelectric (for example, Nano-Mini, Mad City Labs Inc.) and a linear stage (for example, X - stage, model:M-IMS600LM, Newport). The vibrant reflector is connected to the lock-in's sine output through a driver (for example, Nano-Drive, Mad City Labs Inc.). The lock-in controls the piezo-shaker's oscillation frequency (~ 100 Hz), while the driver controls the amplitude. The reflected and transmitted probe-beam crosses through the polarizers (for example, NT47-257, Edmund Optics) whose polarization planes are oriented to reduce the scattered light of the pump-beam, and finally arrives to the photodetectors (for example, FDS1010-CAL, Thorlabs). The electrical signal generated by the photodetectors is low-pass filtered (frequency cut ~ 200 Hz) and detected by the lock-in amplifier (for example, SR830, Stanford Research Systems). Owing to vibrations of the hollow retroreflector, probe-beam has a modulated delay (Fig. (3)).

The constant delay is adjusted by means of x-stage (range of 0 – 1 m, resolution of 3 μm or less) with limits of 0 – 3 ns, resolution of 10 fs. The sine delay depends on piezo-shaker's oscillation (peak to peak movements ranging from 3 μm to 300 μm , resolution of 30 nm, delay of 10 fs - 1 ps, resolution of 0.1 fs) whose amplitude is much lower than constant delay's amplitude.

The probe-beam intensity reflected from the sample have the following components:

- (1) Pulses of duration of femtoseconds (R_p component) which come from the scattered pump-beam whose amplitude is constant.
- (2) Pulse train of reflected probe-beam (ΔR_{DC} component) whose delay is time independent but dependent on x-stage position.
- (3) Pulse train of reflected probe-beam ($\Delta R_{AC}(t)$ component) whose delay is time dependent owing to piezo-shaker's oscillation.

The R_p component is detected by the photodiode after being attenuated by the polarizer. As the photodiode averages the light intensity over time, its output voltage is constant, so this voltage component is not affected by the low-pass filter. Owing that the Lock-in's input works in AC mode, this voltage component is not present in the output. Due to the polarizer, which reduces

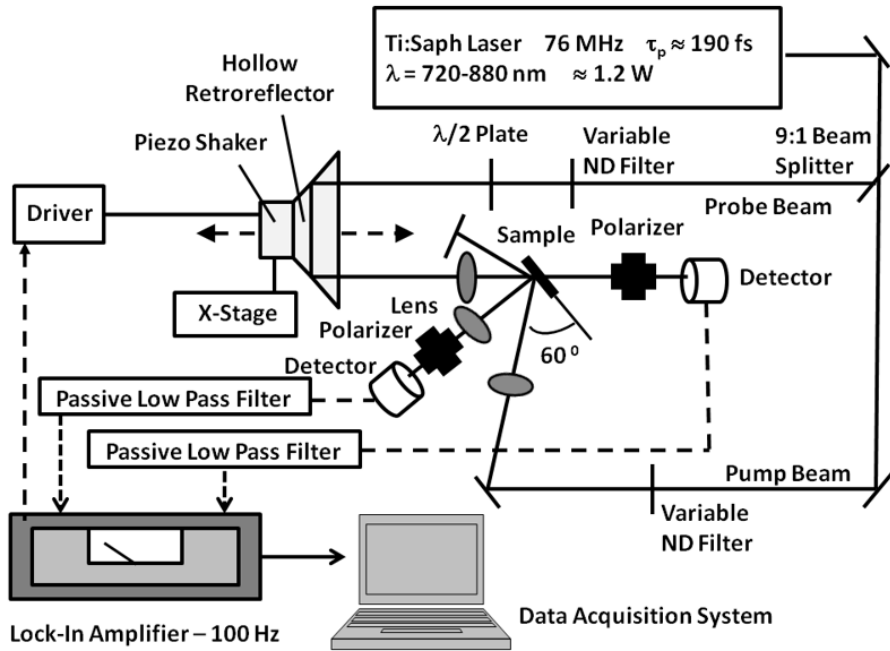


Fig. 2. Experimental setup for the proposed transient thermoreflectance and transient thermodiffusion technique.

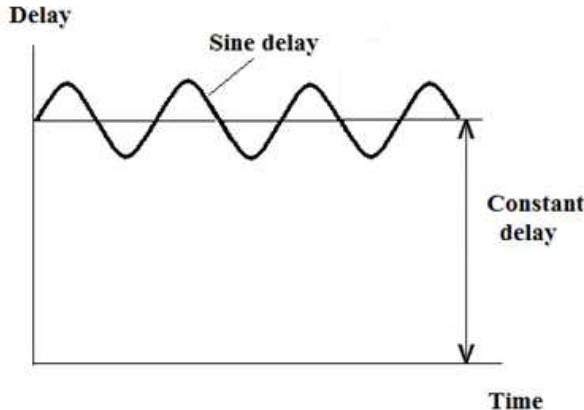


Fig. 3. The total probe-beam delay as a function of the time.

the light intensity, the photodiode is not saturated by R_p component. Similarly, the ΔR_{DC} component, which is not time dependent, is not present in the Lock-in's output.

On the other hand the time dependent $\Delta R_{AC}(t)$ component, makes the photodiode to produce an AC voltage of a given frequency (for example 100 Hz), being this voltage signal present in the Lock-in's output.

The following two points resume the advantages of the proposal: (1) It is possible to have a better time resolution than the pulse width. (2) Noise caused by rough samples can be eliminated.

3. The theory

To theoretically describe our proposal in a simpler manner, we start by supposing that piezo-shaker's movement is performed instantly (not as a sine function). In this way we can represent the time delay as a discrete time series t_i . Owing that Lock-in only detects fundamental harmonic of the signal, this supposition can be applicable. We will also consider only $\Delta R(t)$ graphs (*i.e.* excluding the non-modulated reflection coefficient R). A graph of $\Delta R(t)/R$ is shown in Fig. (4). As laser pulses are Gaussian, we can represent the probe-beam intensity as

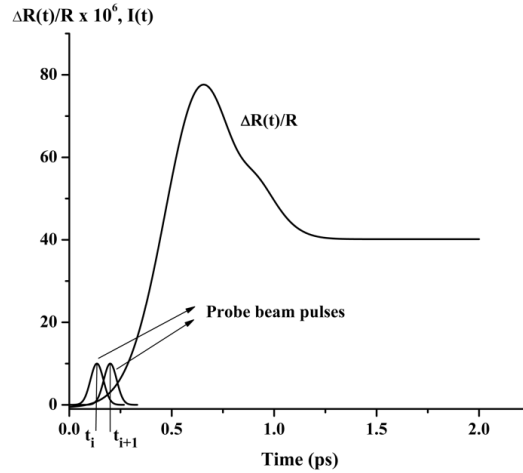


Fig. 4. Reflection coefficient $\Delta R(t)/R$ and the probe-beam for delays t_{i+1} and t_i as a time function (data were taken from Fig. (4) in Ref. [1]).

$$I(t) = A \cdot \exp \left[-\frac{(t - t_0)^2}{2\sigma^2} \right], \quad (1)$$

where t_0 may represent delays t_i or t_{i+1} (Fig. (4)). From now, we will represent intensities at instants t_i and t_{i+1} as $I(t, t_i)$ and $I(t, t_{i+1})$ respectively. Supposing that reflection coefficient is $R + \Delta R(t)$ after probe-beam is reflected by the sample, then reflected light intensities can be represented by

$$I_{R,i}(t) = [R + \Delta R(t)] \cdot I(t, t_i) = R \cdot I(t, t_i) + \Delta R(t)I(t, t_i), \quad (2)$$

$$I_{R,i+1}(t) = [R + \Delta R(t)] \cdot I(t, t_{i+1}) = R \cdot I(t, t_{i+1}) + \Delta R(t)I(t, t_{i+1}). \quad (3)$$

As we can see, first term in right hand of both equations do not change with the time delay so that a DC signal is generated by photodiode which is not detected by Lock-in. On the other hand, second term in right hand of both equations (Fig. (5)) makes the photodiode to produce a time dependent voltage signal which may be represented by

$$V(t) = k \cdot I(t) \quad (4)$$

where k is a constant. Knowing that photodiode averages over time, then voltages produced by this device can be modelled as

$$\overline{V_{R,i}} = k \cdot \left[R \cdot \overline{I(t, t_i)} + \overline{\Delta R(t)I(t, t_i)} \right], \quad (5)$$

$$\overline{V_{R,i+1}} = k \cdot \left[R \cdot \overline{I(t, t_{i+1})} + \Delta R(t) I(t, t_{i+1}) \right]. \quad (6)$$

Figure (5b) shows the voltage produced by photodiode, which is composed by a DC component

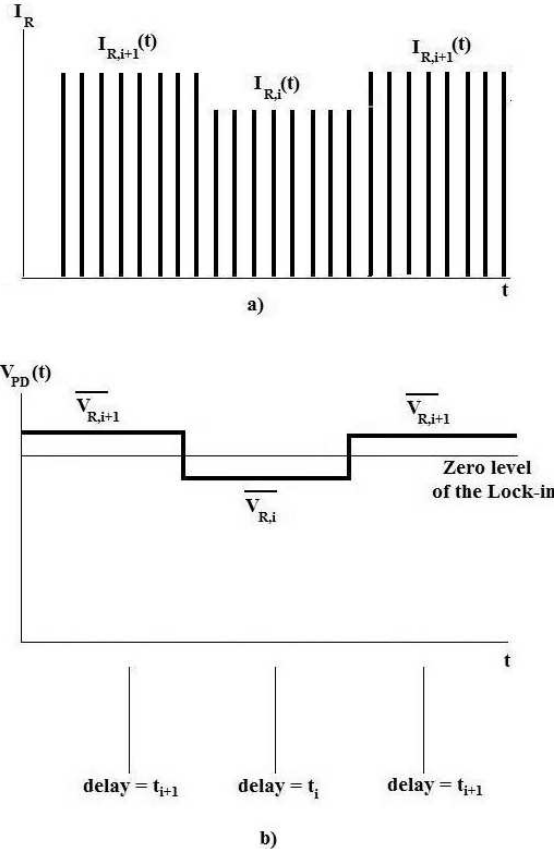


Fig. 5. Reflection coefficient $\Delta R(t)/R$ and the probe-beam for delays t_{i+1} and t_i as a time function (data were taken from Fig. (4) in Ref. [1]).

and a pulse train whose amplitude is synchronized with the frequency of modulation. As Lock-in works in AC mode, it only detects the time dependent voltage V_{DP} whose amplitude is

$$\begin{aligned} Ampl(V_{DP}) &= \overline{V_{R,i+1}} - \overline{V_{R,i}} \\ &= k \cdot \left[\overline{\Delta R(t) I(t, t_{i+1})} - \overline{\Delta R(t) I(t, t_i)} \right] \\ &= k \cdot \overline{\Delta R(t) [I(t, t_{i+1}) - \Delta R(t) I(t, t_i)]}. \end{aligned} \quad (7)$$

Then, Lock-in has an output voltage V_{LI} :

$$V_{LI,i,i+1} = \frac{BkA}{T} \int_0^T \left(\exp \left[-\frac{(t - t_{i+1})^2}{2\sigma^2} \right] - \exp \left[-\frac{(t - t_i)^2}{2\sigma^2} \right] \right) \Delta R(t) dt. \quad (8)$$

Taking in to account that Gauss functions rapidly decreases around the mean, we can rewrite (8) as

$$V_{LI,i,i+1} = \frac{BkA}{T} \int_{-\infty}^{+\infty} \left(\exp \left[-\frac{(t-t_{i+1})^2}{2\sigma^2} \right] - \exp \left[-\frac{(t-t_i)^2}{2\sigma^2} \right] \right) \Delta R(t) dt. \quad (9)$$

4. An algorithm to determine $\Delta R(t)$

4.1. Description of the technique

Although the experimental technique proposed here to analyze energy transport properties in materials may avoid the problems of other already reported techniques, the main drawback is that the signal $\Delta R(t)$ is encoded in $V_{LI,i,i+1}$ (equation (9)). We may define our technique as a translation of an experimental problem to a mathematical one. From the analytical point of view, solving $\Delta R(t)$ from equation (9) may be an extremely difficult problem, however, obtaining a set of measures of $V_{LI,i,i+1}$ and making some approximations, we may develop a numerical algorithm which can give us a good approximation to $\Delta R(t)$.

In order to simplify the notation to explain the following numerical algorithm, we rename the following functions in equation (9): $A(t) = \Delta R(t)$ and $B(t) = V_{LI}$. Also, we suppose that $\frac{BkA}{T} = 1$, and assume that V_{LI} is measured at discrete times t_i , where $i = 1, 2, \dots, m$. On the other hand, establishing that zero mean Gaussian functions are negligible for $|t| > 5\sigma$, and assuming that $t_{i+1} - t_i < 10$ (femtoseconds), then we may approximate (9) with

$$B(t_{i+1}) \approx \int_{t_i-5\sigma}^{t_{i+1}+5\sigma} G_{i+1}(t) A(t) dt, \quad i = 1, 2, \dots, m, \quad (10)$$

where

$$G_{i+1}(t) = \exp \left[-\frac{(t-t_{i+1})^2}{2\sigma^2} \right] - \exp \left[-\frac{(t-t_i)^2}{2\sigma^2} \right]. \quad (11)$$

Let $A(t)$ be represented by a polynomial function, that is,

$$A(t) \approx \sum_{k=0}^L a_k t^k. \quad (12)$$

Now, we may also approximate (9) with

$$B(t_{i+1}) \approx \sum_{k=0}^L a_k \int_{t_i-5\sigma}^{t_{i+1}+5\sigma} G_{i+1}(t) t^k dt. \quad (13)$$

Given that we have a set of data pairs $\left(\sum_{k=0}^L a_k \int_{t_i-5\sigma}^{t_{i+1}+5\sigma} G_{i+1}(t) t^k dt, B(t_{i+1}) \right)$, we may visualize the estimation of coefficients a_k as an optimization problem of the following cost-function

$$U(a_0, a_1, \dots, a_L) = \sum_{i=1}^m \left[\sum_{k=0}^L a_k \int_{t_i-5\sigma}^{t_{i+1}+5\sigma} G_{i+1}(t) t^k dt - B(t_{i+1}) \right]^2. \quad (14)$$

To minimize the square error, we set

$$\frac{\partial U}{\partial a_j} = 2 \sum_{i=1}^m \left[\sum_{k=0}^L a_k \int_{t_i-5\sigma}^{t_{i+1}+5\sigma} G_{i+1}(t) t^k dt - B(t_{i+1}) \right] \int_{t_i-5\sigma}^{t_{i+1}+5\sigma} G_{i+1}(t) t^j dt = 0, \quad (15)$$

for $j = 0, 1, \dots, L$.

Defining $\psi_{i,k} = \int_{t_i-5\sigma}^{t_{i+1}+5\sigma} G_{i+1}(t) t^k dt$ and $\psi_{i,j} = \int_{t_i-5\sigma}^{t_{i+1}+5\sigma} G_{i+1}(t) t^j dt$, we can rewrite (15) as

$$\sum_{i=1}^m \left[\sum_{k=0}^L a_k \psi_{i,k} \right] \psi_{i,j} - \sum_{i=1}^m B(t_{i+1}) \psi_{i,j} = 0. \quad (16)$$

Finally, interchanging the summations and rearranging (16), we obtain

$$\sum_{k=0}^L \left[\sum_{i=1}^m \psi_{i,k} \psi_{i,j} \right] a_k = \sum_{i=1}^m B(t_{i+1}) \psi_{i,j}, \quad j = 0, 1, \dots, L, \quad (17)$$

which represents a simple linear system.

4.2. Numerical experiments

Consider an experiment whose results are like those obtained in Ref. [1], which represent the optical reflection of the surface under test, for example the theoretical graph corresponding to photon wavelength equal to 757 nm (see Ref. [1]). Figure (6) shows the graphs of simulated $A(t_i)$ and $B(t_i)$ for $m = 201$. In this case $t_{i+1} - t_i = 10$ (fs) and $\sigma = \frac{100}{2.35}$ (fs). Figure (6b) shows the graphs of the theoretical and the recovered $A(t_i)$, using the algorithm with $L = 21$.

To evaluate the performance of the algorithm for estimating $A(t_i)$ from the observed data $B(t_i)$,

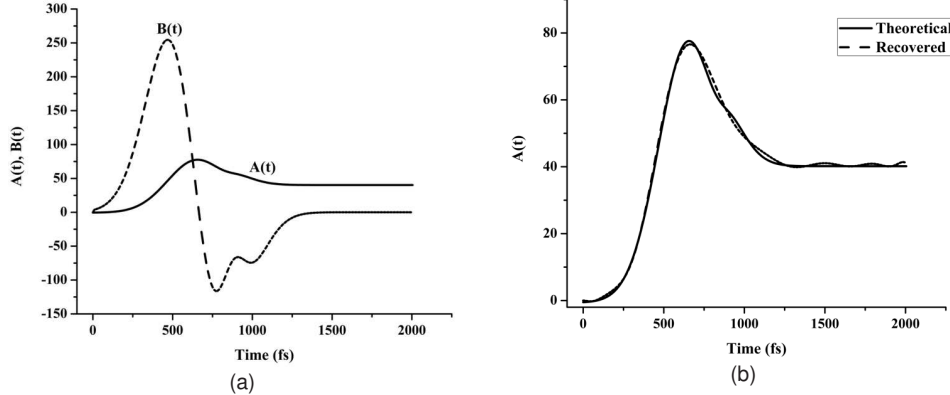


Fig. 6. (a) Theoretical graph of $A(t_i)$ and the graph of $B(t_i)$ computed with equation (10) for $m = 201$. (b) Graphs of the theoretical and recovered $A(t_i)$ for $L = 21$.

it must be established a signal-quality measures by means of an error metrics. In our case, to compare the reconstructed signal with the ideal, we used the normalized root-mean-square error (NRMSE), which is defined as

$$\text{NRMSE} = \sqrt{\frac{\sum |f_t - f_c|^2}{\sum |f_t|^2}} \times 100, \quad (18)$$

where f_t and f_c represent the theoretical and the recovered signal respectively. A better approximation to theoretical $A(t_i)$ depends on the polynomial degree L in equation (13). A simple analysis of the error for several values of L is shown in the graphs of Fig. (7). In Fig. (7a) we can observe that L -NRMSE are not monotonic decreasing graphs, so that a large value

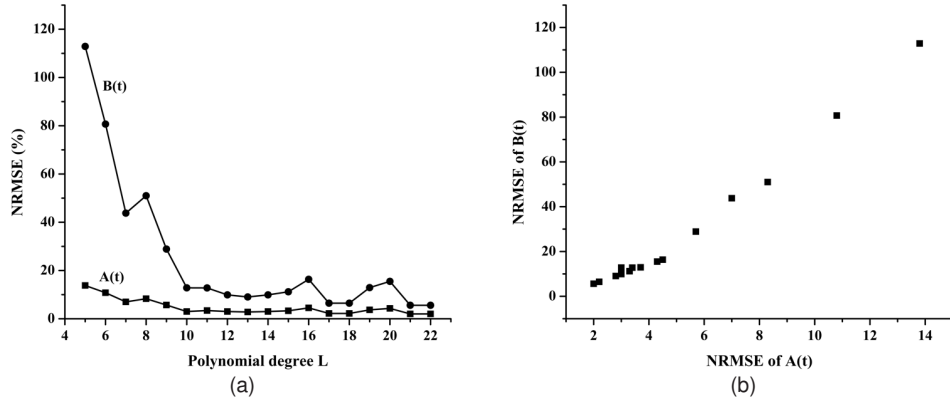


Fig. 7. (a) Graphs of the NRMSE of $A(t_i)$ and $B(t_i)$ for different L values. (b) NRMSE of $A(t_i)$ vs NRMSE of $B(t_i)$ for different L values.

of L does not guarantee a good estimate of $A(t_i)$. In Fig. (7b) we can observe the NRMSE of $A(t_i)$ vs NRMSE of $B(t_i)$ for different L values. Note the correlation between the errors: the curve is monotonic and L values are almost proportional (note that $L = 21$ give us the minimum NRMSE, results of Fig. (6b)).

For the technique to properly work it is necessary to design a criteria to determine an optimal L value. In a real experiment, the only information available is $B(t_i)$, so that once computed $A(t_i)$ for a given L value, we compute $B'(t_i)$ using equation (10), then we use the formula (18) to calculate the NRMSE value of $B'(t_i)$ (compared with $B(t_i)$). This process is performed for several L values (for example, $L = 10, 11, \dots, 22$). Finally, we chose the L value for the minimum NRMSE of $B'(t_i)$, which also corresponds to the minimum NRMSE of $A(t_i)$.

5. Conclusions

We have described an alternative experimental technique for the application of the transient thermoreflectance and transient thermotransmission technique using pump-probe beam examination. We have theoretically demonstrated that our method is free of drawbacks present in already reported techniques. Also, we presented a numerical algorithm to estimate the function $\Delta R(t)/R$ from V_{LI} . We have demonstrated by means of numerical simulations the viability of our algorithm. We also presented a selection criteria for the polynomial degree which allows to estimate $\Delta R(t)/R$ with a minimal NRMSE.

Acknowledgments

We acknowledge the partial support for the realization of this work to the Secretaría de Educación Pública of México through the project PIFI-2010.